Topological Analysis of the Electron Density Distribution in Perturbed Systems. I. Effect of Charge on the Bond Properties of Hydrogen Fluoride

Enrique Espinosa,*,† Ibon Alkorta,‡ Ignasi Mata,§ and Elies Molins§

Laboratoire d'Ingénierie Moléculaire pour la Séparation et les Applications des Gaz, LIMSAG, UMR 5633, Faculté des Sciences Gabriel, Université de Bourgogne, 6 bd. Gabriel, 21100 Dijon, France, Instituto de Química Médica (CSIC), Juan de la Cierva, 3, 28006 Madrid, Spain, and Institut de Ciència de Materials de Barcelona (CSIC), Campus Universitat Autònoma de Barcelona, 08193 Cerdanyola del Vallès, Spain

Received: February 14, 2005; In Final Form: May 31, 2005

Within the framework of the molecular orbital (MO) theory, the addition of one electron to the 4σ antibonding orbital of the neutral (F···H) system or the removal of one electron from its π nonbonding orbitals, leading to $(F\cdots H)^-$ and to $(F\cdots H)^+$, has permitted the investigation of these charge perturbations on the bond properties of the hydrogen fluoride molecule by using the topological analysis of $\rho(\mathbf{r})$. For (F···H), $(F\cdots H)^-$, and $(F\cdots H)^+$, the topological and energetic properties calculated at the F···H bond critical point (BCP) have been related to the 3σ bonding molecular orbital (BMO) distribution, as this orbital is the main contributor to $\rho(\mathbf{r})$ at the interatomic surface. The analysis has been carried out at several F···H internuclear distances, ranging from 0.8 to 3.0 Å. As far as the BMO distribution results from its interaction with the average Coulomb and exchange potential generated by the charge filling the other MOs, and in particular by the π and 4σ electrons, the comparison between the BCP properties calculated for the charged systems and those corresponding to the neutral one permits the interpretation of the differences in terms of the charge perturbation on BMO. Along with the BCP properties of (F···H), $(F\cdots H)^-$, and $(F\cdots H)^+$, the interaction energy magnitudes of these systems have been also calculated within the same range of internuclear distances, indicating that the applied perturbations do not break the F−H bond but soften it, giving rise to the stable species $(F-H)^-$ and $(F-H)^+$. Comparing the three systems at their equilibrium geometries, the most stable configuration, which corresponds to the unperturbed (F···H) system, shows the highest quantity and the most locally concentrated charge density distribution, along with the largest total electron energy density magnitude, at the interatomic surface as a consequence of the BMO contraction toward the fluorine nucleus in $(F\cdots H)^+$ and of the BMO expansion toward both nuclei in $(F\cdots H)^-$. On the other hand, if the comparison is carried out at the equilibrium distance of (F···H) (d_{eq}^0), this one exhibits both the smallest total energy density magnitude and the largest quantity of bonding charge at the interatomic surface. Hence, being the signature of the most stable configuration, the characteristic magnitudes of the neutral system $\rho(d_{eq}^0)$, $\nabla^2\rho(d_{eq}^0)$, and $H(d_{eq}^0)$ appear as boundary conditions at the interatomic surface of its unperturbed and relaxed electron distribution.

1. Introduction

From the quantum mechanics theory, the physical and chemical properties of a material are related to the wave function of the system. The appearance of the density functional theory reduced this strong requirement and demonstrated that knowledge of the electron distribution is enough for deducing the materials behavior.[1−3] The electron density in solids can be separated in two parts, namely inner and valence atomic shells. While atomic inner shells are dominated by strong interactions with nuclei, the valence shells are easily affected by the environment, regarded at (i) other atoms or ions, (ii) crystal or external fields, or (iii) any other perturbation. Although most of spectroscopic techniques give insight of valence states, the most fruitful ways to reach their precise electron density distribution $\rho(\mathbf{r})$ are computational quantum methods and accurate diffraction experiments.

The "atoms in molecules" (AIM) methodology[4] allows the characterization of interatomic interactions by using the topological analysis of $\rho(\mathbf{r})$. Within this methodology, atomic basins are separated by zero flux surfaces $S(\mathbf{r})$ of $\rho(\mathbf{r})$ ($\nabla\rho(\mathbf{r})\cdot\mathbf{n}(\mathbf{r}) = 0$, $\forall\mathbf{r} \in S(\mathbf{r})$, $\mathbf{n}$ being the unit vector orthogonal to S at $\mathbf{r}$) and the bond critical points (BCPs) are defined as the saddle points of the $\rho(\mathbf{r})$ distribution at the interatomic surfaces $S(\mathbf{r})$ ($\nabla\rho(\mathbf{r}_{BCP}) = 0$, $\mathbf{r}_{BCP} \in S$). In a series of papers,[5−10] we have shown that the topological properties evaluated at BCPs can be regarded as boundary conditions in the electron density distribution that, if it does not completely define the system, at least they introduce a very important constraint on the possible distributions. We have also observed that there are direct relationships connecting topological and energetic properties of the electron density at BCPs. Moreover, exponential dependencies of topological and energetic properties at BCPs on the internuclear distance have been shown for the closed- and shared-shell regimes.

The experimental availability and the small size of the FH molecule have allowed the careful characterization of the spectroscopic properties for the neutral and charged species

* To whom correspondence should be addressed. E-mail: Enrique.Espinosa@u-bourgogne.fr.
† Université de Bourgogne.
‡ CSIC, Madrid, Spain.
§ CSIC, Cerdanyola del Vallès, Spain.

10.1021/jp050776s CCC: $30.25
Published on Web 07/01/2005

(cation and anion).[11,12] It has been used as a test case for the validation of a number of theoretical developments on (i) the analysis of the electron distribution and energetics within the AIM methodology,[13−15] (ii) the ELF (electron localization function) description of its polar bond,[16] (iii) hydrogen bonding properties,[17] (iv) atomic charge comparison between different partition methods,[18] and (v) dynamic polarizabilities,[19] etc. In our research, the F···H system and several neutral, positively, and negatively charged X−H···F−Y complexes have been studied to some extent.[10] From this work, the dependences of the topological and energetic properties calculated at the F···H BCP over a long range of internuclear distances have been characterized from long hydrogen bonding geometries to short covalent ones.

More knowledge in the relationship between these BCP properties and the chemical bond can be obtained by the study of perturbed systems. With this aim we have analyzed the influence of a total unbalanced charge in the hydrogen fluoride molecule, as either one-electron addition to or one-electron removal from the neutral (F···H) system, by means of the evaluation of the $(F\cdots H)^-$, $(F\cdots H)^+$, and (F···H) BCP properties from long to short internuclear geometries. The calculated properties were the electron density (ρ^{BCP}), the Laplacian of the electron density ($\nabla^2\rho^{BCP}$), the perpendicular (λ_1^{BCP}, λ_2^{BCP}), and the parallel (λ_3^{BCP}) curvatures with respect to the bond path direction, and the local kinetic (G^{BCP}), potential (V^{BCP}), and total (H^{BCP}) energy densities. In the following discussion the superscripts $^-$, $^+$, and ^{0} identify the $(F\cdots H)^-$, $(F\cdots H)^+$, and (F···H) systems, respectively. In addition, as far as all topological and local energetic properties analyzed in this work have been calculated at the bond critical point, hereafter we will omit the superscript BCP for clarity. Along with the BCP properties, we have also characterized the interaction energy dependences of these systems on the F···H distance.

2. Calculations

For an adequate description of the wave function in a broad range of interatomic distances, multireference CASSCF (complete active space self-consistent field)[20] calculation with the 6-311++G** basis set has been carried out. All the valence electrons (eight, seven, and nine in the neutral, positively, and negatively charged systems, respectively) and eight orbitals as active space have been considered. The wave function has been optimized with the GAMESS program.[21] The dissociation of the systems produces the neutral atoms for (F···H), the neutral fluorine atom and a proton for $(F\cdots H)^+$, and the negatively charged fluorine and the neutral hydrogen for $(F\cdots H)^-$. The BCP properties and interaction energies calculated for the three systems within the 0.8−3.0 Å range of F···H distances are given as Supporting Information.

3. Molecular Orbitals and Equilibrium Geometries

In the framework of the molecular orbital (MO) theory, the neutral (F···H) molecule in the ground state is represented by the configuration $(1\sigma)^2(2\sigma)^2(3\sigma)^2(1\pi)^2(2\pi)^2(4\sigma)^0$, where all but 1σ are MOs involving valence electrons. Accordingly, while the vertical ionization of the system leads to $(F\cdots H)^+$ by removing one electron from the π nonbonding orbitals, the $(F\cdots H)^-$ system is obtained by adding one electron to the 4σ antibonding orbital.

To understand the influence of the charge perturbation on the BCP properties, several points should be stressed. First, (i) the F···H internuclear direction lies on the nodal planes of the π nonbonding orbitals and (ii) the 4σ nodal plane cuts orthogonally in that direction very close to the interatomic surface (Figure 1). As a consequence, the π and 4σ electron distributions cannot directly contribute to $\rho(\mathbf{r})$ at BCP, which mainly accounts for the participation of the 1σ and 2σ nonbonding orbitals and the 3σ bonding molecular orbital (BMO), because they recover the F···H internuclear region and therefore BCP. However, since the 1σ and 2σ MOs are respectively built from the 1s and mainly from the 2s fluorine electrons, which are the deepest in energy for the three systems, the dependences of their distributions on the internuclear distance and on the charge perturbation will not be as important as that of the 3σ BMO, and the latter will be therefore considered as the main contributor to the dependences observed for the BCP properties. In particular, the self-consistency property of the electronic structure, implying that each orbital is determined by its interaction with the average Coulomb and exchange potential generated by electrons in other occupied orbitals, leads to the obvious conclusion that the BMO electron distribution is not independent from these of the π and 4σ MOs. Hence, when comparing the BCP properties calculated for the charged systems to those of the neutral one, the differences will be interpreted in terms of their BMO electron distributions as resulting from the perturbations associated to either the one-electron removal from the π nonbonding orbitals or the one-electron addition to the 4σ antibonding orbital.

The three selected systems are stable species with different equilibrium distances $d_{eq}^0 < d_{eq}^- < d_{eq}^+$ (Table 1). This classification indicates that either adding or removing one electron from the neutral system lengthens the bond and therefore points to a softening of the F···H interaction as shown by the calculated interaction energies at these geometries (Table 1). While $d_{eq}^0 < d_{eq}^-$ is in accord with the predictions of the MO theory when one electron is added to an antibonding orbital,[22,23] the fact that $(F\cdots H)^+$ exhibits the largest equilibrium distance among the three systems is an unexpected result taking into account that the removed electron is coming from a nonbonding orbital. This particular behavior is interpreted in terms of the high electronegativity of fluorine compared to that of hydrogen. Thus, as a consequence of ionization, the bonding charge is attracted by fluorine, leading to a contraction of BMO that (i) reduces the electron density distribution at the interatomic surface and (ii) induces an effective weakening of the interaction. Indeed, inspection of the BMO populations (NBO method) shows that the total bonding charge does not significantly vary from (F···H) to $(F\cdots H)^+$ ($q^0 = 1.979\ e$ and $q^+ = 1.981\ e$ at their respective equilibrium distances), indicating that $d_{eq}^0 < d_{eq}^+$ is not due to a diminution of the BMO population (we observe the expected population of $\cong 3\ e$ for the π nonbonding orbitals of $(F\cdots H)^+$). In addition, the calculation of the relative position of BCP with respect to the middle of the equilibrium geometry ($\Delta_{eq} = [d(F\cdots BCP) - d(F\cdots H)/2]/d(F\cdots H)$) for both (F···H) and $(F\cdots H)^+$ ($\Delta_{eq}^0 = 34.0\%$ and $\Delta_{eq}^+ = 35.9\%$) points to the expansion of the fluorine atomic basin in $(F\cdots H)^+$, which corresponds to the contraction of BMO toward the F-nucleus and the concomitant diminution of the electron density at the interatomic surface $\rho^+(d_{eq}^+) < \rho^0(d_{eq}^0)$ (Table 1). In the case of $(F\cdots H)^-$, the value $\Delta_{eq}^- = 34.0\%$ indicates that, compared to the neutral system, the relative position of BCP does not change and, going from (F···H) to $(F\cdots H)^-$, the classification $d_{eq}^0 < d_{eq}^-$ should be associated with an expansion of BMO toward both nuclei in $(F\cdots H)^-$. Because the BMO populations are not significantly different ($q^0 = 1.979\ e$ and $q^- = 1.981\ e$), the observed BMO expansion should be responsible for the

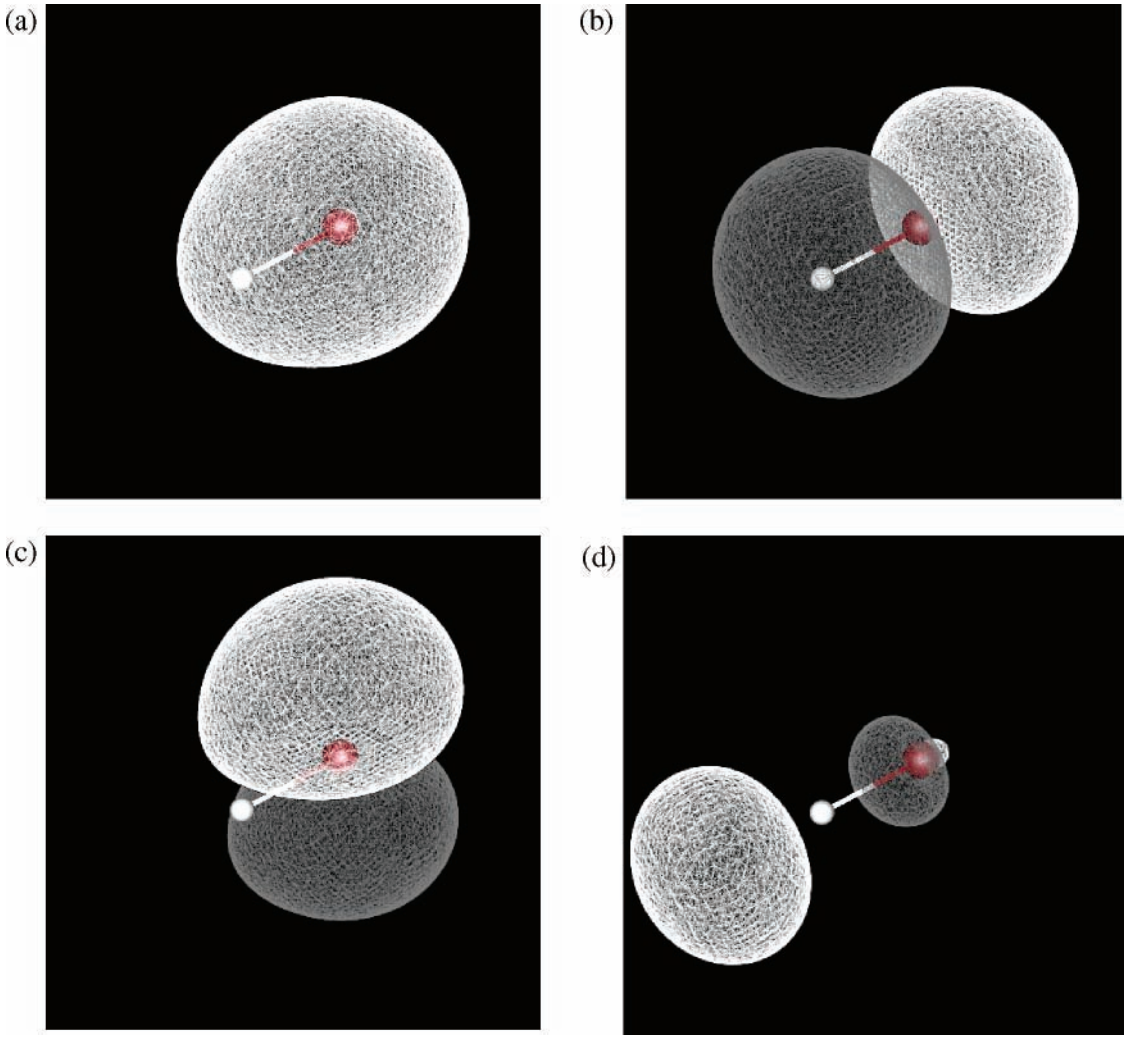

Figure 1. Molecular orbitals of the neutral (F···H) system at the equilibrium geometry: (a) 2σ, (b) 3σ, (c) 1π, and (d) 4σ. Fluorine and hydrogen atoms are represented in red and white colors, respectively. The 2π MO, not shown here, possesses the same energy as 1π and can be represented by rotating the latter 90° clockwise around the internuclear direction F···H. Within a cubic grid of $80 \times 80 \times 80$ points, the 4σ nodal plane is found to cut the internuclear direction at 0.786 Å from the F-nucleus, and therefore it is separated 0.015 Å from the BCP position. In the neutral system, the 4σ antibonding MO is empty and represents the LUMO. All MOs have been plotted using the same constant value (0.05) for the wave function.

diminution of the electron density along the internuclear region of the negatively charged system, and therefore for $\rho^-(d_{eq}^-) < \rho^0(d_{eq}^0)$. According to the BMO^0, BMO$^+$, and BMO$^-$ polarizations, the local concentration of the electron density ($\nabla^2\rho$) and the total energy density (H) magnitudes exhibit similar classifications than this found for ρ ($\rho^0(d_{eq}^0) > \rho^-(d_{eq}^-) > \rho^+(d_{eq}^+)$, $|\nabla^2\rho^0(d_{eq}^0)| > |\nabla^2\rho^-(d_{eq}^-)| > |\nabla^2\rho^+(d_{eq}^+)|$, $|H^0(d_{eq}^0)| > |H^-(d_{eq}^-)| > |H^+(d_{eq}^+)|$), indicating that the most stable electron configuration (i.e., that corresponding to the unperturbed system) shows (i) the largest quantity, (ii) the most locally concentrated, and (iii) the deepest energetically stabilized bonding charge distribution at the interatomic surface.

On the other side, comparing the systems at d_{eq}^0, we observe that while the most stable configuration still exhibits the largest ρ magnitude, that is no longer the case for $\nabla^2\rho$ and H (Table 1). Indeed, at this geometry, the fluorine basin expands in both (F···H)$^+$ and (F···H)$^-$ when compared to the F-basin of the neutral system ($\Delta^+(d_{eq}^0) = 36.7\%$, $\Delta^-(d_{eq}^0) = 34.4\%$, and $\Delta^0(d_{eq}^0) = 34.0\%$) and also to their corresponding F-basins at their equilibrium geometries ($\Delta^+(d_{eq}^+) = 35.9\%$ and $\Delta^-(d_{eq}^-) = 34.0\%$). Accordingly, the BMO of the charged systems at d_{eq}^0 is more contracted toward the fluorine nucleus, and therefore the interatomic surface expands toward the hydrogen nucleus in both cases. Thus, as a consequence of a longer d_{eq}^0(F···BCP) distance in the perturbed systems (d_{eq}^0(F···BCP) = 0.796, 0.775, and 0.771 Å for (F···H)$^+$, (F···H)$^-$, and (F···H), respectively), the repulsive interaction between the electron distribution at the interatomic surface and that accumulated around the fluorine nucleus is weaker for (F···H)$^+$ and (F···H)$^-$ than for (F···H) at d_{eq}^0, leading to a stabilization of the electron distribution at the interatomic surface of the charged systems ($H^+(d_{eq}^0) < H^-(d_{eq}^0) < H^0(d_{eq}^0)$), which shows as a function of d_{eq}^0(F···BCP). In addition, while the bonding charge is more concentrated in (F···H)$^+$ than in (F···H) ($\nabla^2\rho^+(d_{eq}^0) < \nabla^2\rho^0(d_{eq}^0)$), mirroring a weaker repulsive interaction in the former case due to a fewer quantity of π nonbonding electrons, the bonding electron distribution is similarly concentrated in both (F···H) and (F···H)$^-$ ($\nabla^2\rho^0(d_{eq}^0) \approx \nabla^2\rho^-(d_{eq}^0)$) because the latter system compensates the additional repulsive interaction due to the extra electron by contracting BMO toward the fluorine basin, therefore leading to a fewer quantity of charge at the interatomic surface ($\rho^-(d_{eq}^0) < \rho^0(d_{eq}^0)$).

To show up the characteristic BMO polarization along the F···H internuclear region for (F···H)$^+$, (F···H)$^-$, and (F···H)$^-$, we have represented the dependences of the Δ^+, Δ^-, and Δ^0 magnitudes on the F···H distance in Figure 2. For all systems,

TABLE 1: Selected BCP Topological and Energetic Properties of the $(F\cdots H)^+$, $(F\cdots H)$, and $(F\cdots H)^-$ Systems Calculated at Their Equilibrium Geometries (d_{eq}) and at the Equilibrium Geometry of the Neutral System (d_{eq}^0)[a]

	$(F\cdots H)^+$	$(F\cdots H)$	$(F\cdots H)^-$
d_{eq}	0.999	0.918	0.941
$d_{eq}(F\cdots BCP)$	0.858	0.771	0.790
$d_{eq}^0(F\cdots BCP)$	0.796	0.771	0.775
$E_{int}(d_{eq})$	−335.7	−578.4	−150.5
$\rho(d_{eq})$	1.78	2.50	2.28
$\rho(d_{eq}^0)$	2.33	2.50	2.45
$\nabla^2\rho(d_{eq})$	−52.5	−69.3	−61.3
$\nabla^2\rho(d_{eq}^0)$	−86.8	−69.3	−69.2
$H(d_{eq})$	−10256	−14302	−12720
$H(d_{eq}^0)$	−16892	−14302	−14316
$d(\nabla^2\rho=0)$	2.80	1.60	1.35
$d(H=0)$	2.83	1.95	2.50
$d(\nabla^2\rho_{max})$	2.97	1.90	1.60
$\nabla^2\rho_{max}$	<0.01	1.1	2.8

[a] For each system, $d_{eq}(F\cdots BCP)$ and $d_{eq}^0(F\cdots BCP)$ represent the distance from the fluorine nucleus to the BCP position at its equilibrium geometry and at d_{eq}^0, respectively. E_{int} represents the interaction energy of the system. The characteristic distances $d(H=0)$ and $d(\nabla^2\rho=0)$ define the boundaries between regions I and II and between regions II and III, and $d(\nabla^2\rho_{max})$ is the geometry corresponding to the maximum Laplacian value $\nabla^2\rho_{max}$, which exhibits in region II for $(F\cdots H)$ and $(F\cdots H)^-$ and in region I for $(F\cdots H)^+$. Units are as follows: d, Å; d_{eq}, Å; ρ, e/Å^3; $\nabla^2\rho$, e/Å^5; H, (kJ/mol)/Å^3; E_{int}, kJ/mol.

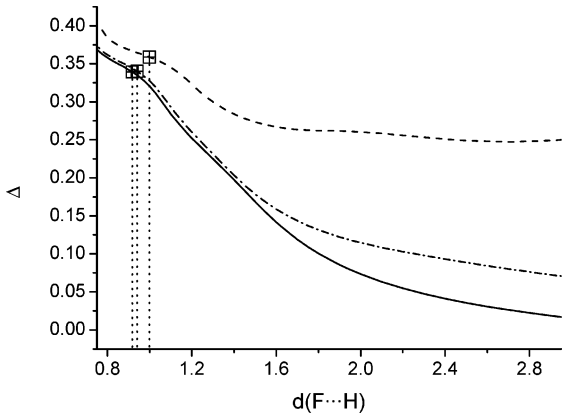

Figure 2. Δ dependence on $d(F\cdots H)$ (Å) for the $(F\cdots H)^+$ (--), $(F\cdots H)$ (—), and $(F\cdots H)^-$ (− · −) systems. Δ is defined as the relative position of BCP with respect to the middle of the internuclear distance: $\Delta = [d(F\cdots BCP) - d(F\cdots H)/2]/d(F\cdots H)$. Target points correspond to the values observed at the equilibrium geometries $d_{eq}^0 < d_{eq}^- < d_{eq}^+$ (Table 1).

Δ values rise from long to short geometries, indicating a monotonic BMO contraction toward fluorine. The calculated Δ^+ magnitudes are significantly larger than those of Δ^- and Δ^0 , reflecting the more important BMO contraction in the former system for all distances. In particular, as a consequence of the $(F\cdots H)^+$ dissociation in the neutral fluorine and a proton, the high Δ^+ values at long geometries (25%) do not tend toward zero as those of Δ^- and Δ^0 do (7 and 2%, respectively). Moreover, the most important differences between Δ^- and Δ^0 show for closed-shell interactions ($\nabla^2\rho > 0$, $d > d(\nabla^2\rho=0)$; see Table 1), where $\Delta^- > \Delta^0$ indicates that the additional contraction of BMO^- compared to that of BMO^0 is due to the extra electron in the former system when the bonding orbital is not still completely formed.[10] For shared-shell interactions ($\nabla^2\rho < 0$, $d < d(\nabla^2\rho=0)$), the bonding orbital is formed in both cases and the systems exhibit very small differences ($\Delta^- \sim \Delta^0$).

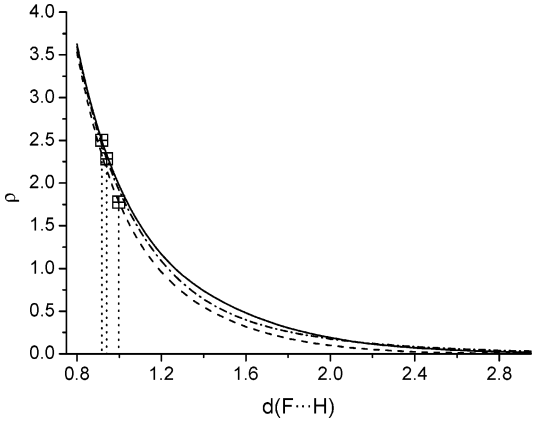

Figure 3. ρ dependence on $d(F\cdots H)$ for the $(F\cdots H)^+$ (--), $(F\cdots H)$ (—), and $(F\cdots H)^-$ (− · −) systems. Units are in e/Å^3 and in Å, respectively. Target points correspond to the values observed at the equilibrium geometries $d_{eq}^0 < d_{eq}^- < d_{eq}^+$ (Table 1).

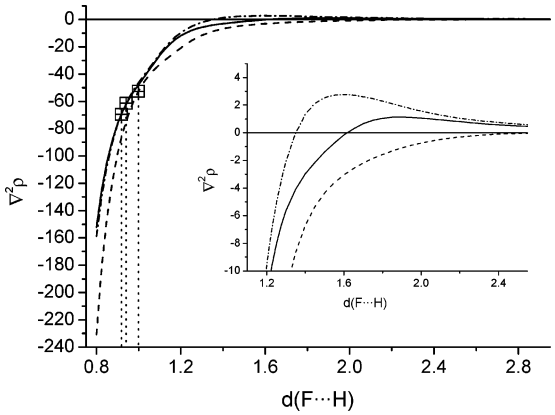

Figure 4. $\nabla^2\rho$ dependence on $d(F\cdots H)$ for the $(F\cdots H)^+$ (--), $(F\cdots H)$ (—), and $(F\cdots H)^-$ (− · −) systems. Units are in e/Å^5 and in Å, respectively. Target points correspond to the values observed at the equilibrium geometries $d_{eq}^0 < d_{eq}^- < d_{eq}^+$ (Table 1).

4. Topological Properties at the Bond Critical Point

Figure 3 shows the BCP electron density magnitudes calculated for the three systems within the range of internuclear distances of 0.8−3.0 Å. While the highest density corresponds to the neutral system (ρ^0), the lowest is observed for the positively charged one (ρ^+). The dependences observed for the three systems appear to be very similar, the largest difference being 0.21 e Å^{-3} at $d = 1.1$ Å. This variation corresponds to 14% of the ρ^0 value at this distance. The perturbations on BMO lead to the classification $\rho^0 > \rho^- > \rho^+$ within the full range of distances but do not significantly affect the dependence of ρ on the internuclear distance. In this way, the differences observed among the $\rho^0(d_{eq}^0)$, $\rho^-(d_{eq}^-)$, and $\rho^+(d_{eq}^+)$ magnitudes are mostly due to the displacement of the equilibrium position. Thus, as a consequence of both the observed classification $d_{eq}^0 < d_{eq}^- < d_{eq}^+$ and the exponential dependence of ρ on the internuclear distance in the shared-shell region,[10] we found $\rho^0(d_{eq}^0) > \rho^-(d_{eq}^-) > \rho^+(d_{eq}^+)$. In particular, the decreasing of ρ with the addition of one antibonding electron is in agreement with previous works.[24]

A different aspect appears when representing the $\nabla^2\rho$ magnitudes calculated for the three systems in the same range of distances (Figure 4). In this case, the dependence of the neutral system is intermediate between those of the charged ones. According to the behavior observed for $(F\cdots H)$,[10] the whole range of interactions can be divided in three regions. From

long to short geometries, they correspond to *pure* closed-shell (region I), intermediate closed-shell (region II), and shared-shell (region III) interactions. The boundaries between regions I and II and between regions II and III are associated with the internuclear distances $d(H=0)$ and $d(\nabla^2\rho=0)$, respectively (see Table 1).

The negatively charged system behaves qualitatively similar to the neutral one, but region II is more extended and the peak at $\nabla^2\rho_{max}$ is more pronounced and displaced to a shorter distance in $(F\cdots H)^-$. On the other side, $(F\cdots H)^+$ shows a very different behavior, with region III extending to very large distances and exhibiting a very small region II. According to the expected asymptotic dependence of $\nabla^2\rho$ in region I ($\nabla^2\rho \rightarrow 0$ for $d \rightarrow \infty$) and to the positive $\nabla^2\rho$ magnitudes shown in regions I and II, a local maximum should be found in region II.[10] However, while that is the case for $(F\cdots H)$ and $(F\cdots H)^-$, no local maximum was observed for $(F\cdots H)^+$ within the considered range of distances. The calculation of $\nabla^2\rho^+$ by using a small enough grid of internuclear distances leads to the appearance of a very flat local maximum in region I ($\nabla^2\rho_{max}{}^+ = 0.0023$ e Å^{-5} at $d = 2.97$ Å), which is significantly lower than $\nabla^2\rho_{max}{}^0 = 1.14$ e Å^{-5} and $\nabla^2\rho_{max}{}^- = 2.76$ e Å^{-5} at $d = 1.90$ and 1.60 Å, respectively.

On the other hand, in the case of the X−H···F−Y complexes,[10] the $d^+ < d^0 < d^-$ classification observed for each characteristic distance (namely, $d(\nabla^2\rho=0)$, $d(H=0)$, and $d(\nabla^2\rho_{max})$), as well as that found for the maximum Laplacian values $(\nabla^2\rho_{max})^+ > (\nabla^2\rho_{max})^0 > (\nabla^2\rho_{max})^-$, are different from those shown here (except for $d^0(H=0) < d^-(H=0)$). Indeed, as a consequence of the absence of the X and Y chemical groups in the actual systems, the charge perturbation applied on the (H···F) neutral system strongly affects its bonding distribution. In the case of X−H···F−Y complexes, however, the X and Y groups permit partially absorbtion of this perturbation as a function of their electronegativity, modulating the BCP properties. Hence, the different classification observed for the characteristic distances and the Laplacian plots of the X−H···F−Y complexes seem to be related to a polarization effect induced by the X and Y groups, which cannot take place in the systems treated here.

In the range of 0.8−1.1 Å, while the positively charged system gives rise to a faster increase of the negative Laplacian magnitude when approaching the nuclei, ρ tends to be closer between the three systems. In that range of internuclear distances, which belongs to region III and where we find d_{eq} for the three cases, the relative differences between the extreme Laplacian curves can be significant. For instance, at the equilibrium geometry of the neutral (F···H) system ($d_{eq}{}^0 = 0.918$ Å) we observe $\Delta(\nabla^2\rho(d_{eq}{}^0)) = [\nabla^2\rho^0(d_{eq}{}^0) - \nabla^2\rho^+(d_{eq}{}^0)]/\nabla^2\rho^0(d_{eq}{}^0) = 25\%$. Therefore, in contrast to $\rho(d_{eq})$, the differences between the $\nabla^2\rho(d_{eq})$ magnitudes calculated for the three systems are not only due to the displacement of the equilibrium distance but also to changes in the dependence of this topological property.

The Laplacian magnitude at BCP can be decomposed in positive (λ_3) and in negative (λ_1 and λ_2) components ($\nabla^2\rho = \lambda_1 + \lambda_2 + \lambda_3$), which are the parallel and the perpendicular curvatures of $\rho(\mathbf{r})$ to the bond path direction, respectively. Their dependences on the F···H internuclear distance are shown in Figure 5. While the magnitudes of the perpendicular curvatures are very similar among the three systems, that is not the case for λ_3, in particular for intermediate geometries. This feature points to the differences observed in the dependences of the parallel curvatures $\lambda_3{}^0$, $\lambda_3{}^+$, and $\lambda_3{}^-$ as being at the origin of

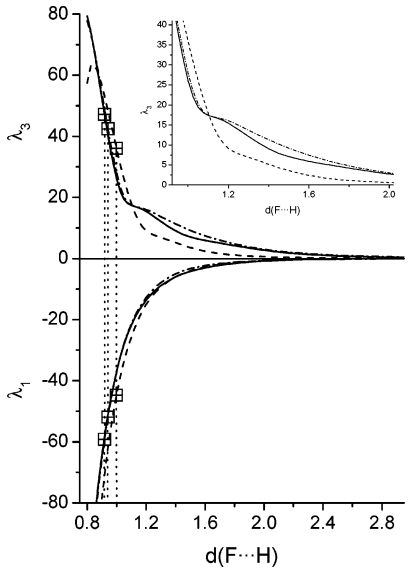

Figure 5. λ_3 (positive values) and λ_1 (negative values) dependence on d(F···H) distance for the $(F\cdots H)^+$ (--), (F···H) (—), and $(F\cdots H)^-$ ($-\cdot-$) systems. $\lambda_1 = \lambda_2$ due to the cylindrical symmetry along the bonding direction. Units are in e/Å^5 and in Å, respectively. Target points correspond to the values observed at the equilibrium geometries $d_{eq}{}^0 < d_{eq}{}^- < d_{eq}{}^+$ (Table 1).

the corresponding ones in the Laplacian magnitudes. The behaviors observed for $\lambda_3{}^0$ and $\lambda_3{}^-$ are very similar, showing an exponential decrease with an elbow within the range of 1.1−1.4 Å, appearing more pronounced for $\lambda_3{}^-$. The dependence observed for $\lambda_3{}^+$ shows no elbow and crosses the other two at $d = 1.1$ Å, exhibiting larger values than those of $\lambda_3{}^0$ and $\lambda_3{}^-$ in the range of $0.85 < d < 1.1$ Å, where a local maximum in $\lambda_3{}^+$ appears. This maximum, shown at $d \sim 0.9$ Å, could be related to the fluorine inner-shell contribution at BCP. Thus, a starting 2σ dependence on d(H···F) could be responsible for the observed $(\lambda_3{}^+)_{max}$, as resulting from the addition of the actual 2σ contribution to that of BMO.

Even if a close similarity is observed for the curvatures of the negatively charged and neutral systems, the balance between their positive and negative contributions to $\nabla^2\rho$ leads to $\nabla^2\rho^0 < \nabla^2\rho^-$ for a large range of internuclear distances ($d > 0.925$ Å). The addition of one electron to the neutral (F···H) system produces the increase of the charge depletion in the bonding region, as shown by $\lambda_3{}^0 < \lambda_3{}^-$ and by $|\lambda_1{}^-| < |\lambda_1{}^0|$ for $d > 0.925$ Å and $d > 1.025$ Å, respectively. This effect of charge, which also explains the decrease of the ρ magnitude observed for $(F\cdots H)^-$ when compared to (F···H), mirrors the loss in stabilization of BMO and correlates with the electron configuration of the $(F\cdots H)^-$ system, where the unbalanced electron, placed in the 4σ antibonding orbital, weakens the bond. On the other side, as a result of a fewer number of electrons in $(F\cdots H)^+$ and the subsequent weakening in the repulsion between them, the charge appears, in this case, more concentrated ($\nabla^2\rho^+ < \nabla^2\rho^0$) for all distances (here shown by $|\lambda_1{}^0| < |\lambda_1{}^+|$ and by $\lambda_3{}^+ < \lambda_3{}^0$ for $d < 1.35$ Å and for $d > 1.125$ Å, respectively). In this case, however, even if the $(F\cdots H)^+$ bonding charge is more concentrated at the interatomic surface, the decrease in magnitude of ρ ($\rho^+ < \rho^0$) as a consequence of the more important BMO^+ polarization, also weakens the bond ($d_{eq}{}^+ > d_{eq}{}^0$).

The range of intermolecular geometries associated with the (F···H) bonding molecular orbital formation has been identified as that of region II (i.e., $d(\nabla^2\rho=0) < d < d(H=0)$).[10] Hence, the additional electron in $(F\cdots H)^-$ would favor the formation

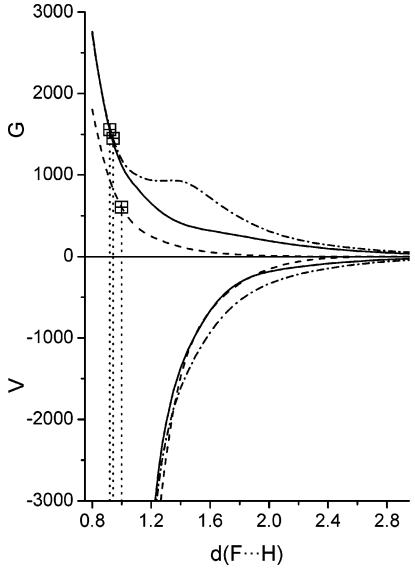

Figure 6. G (positive values) and V (negative values) dependence on d(F···H) for the $(F\cdots H)^+$ (--), (F···H) (—), and $(F\cdots H)^-$ (– · –) systems. Units are in (kJ/mol)/Å^3 and in Å, respectively. Target points correspond to the values observed at the equilibrium geometries $d_{eq}{}^0 < d_{eq}{}^- < d_{eq}{}^+$ (Table 1).

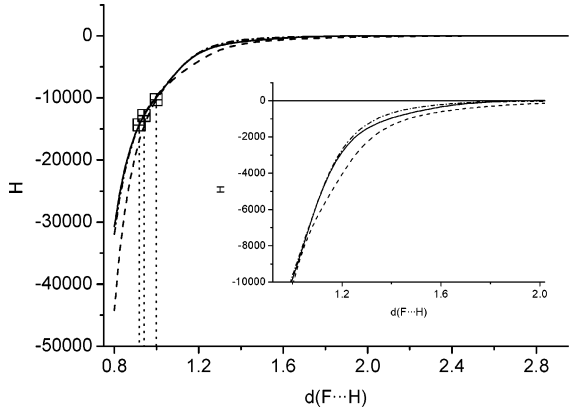

Figure 7. H dependence on d(F···H) for the $(F\cdots H)^+$ (--), (F···H) (—), and $(F\cdots H)^-$ (– · –) systems. Units are in (kJ/mol)/Å^3 and in Å, respectively. Target points correspond to the values observed at the equilibrium geometries $d_{eq}{}^0 < d_{eq}{}^- < d_{eq}{}^+$ (Table 1).

of the bonding orbital at larger distances than in the neutral case (see Table 1). Shortening the internuclear distance the interaction between the charge filling the 4σ and 3σ orbitals would hinder, however, the population of the latter, extending region II to shorter distances than in the neutral case and producing the observed enlargement of region II for $(F\cdots H)^-$.

In $(F\cdots H)^+$ the removal of one electron from the π nonbonding orbitals produces qualitative differences in the behavior of this system. Thus, region II involves an extremely short range of geometries at long intermolecular distances ($2.80 < d < 2.83$ Å), indicating both an earlier and a faster formation of the bonding molecular orbital than for the two other systems (F···H) and $(F\cdots H)^-$. Moreover, the neutral H-atom produced in the dissociation of (F···H) and $(F\cdots H)^-$ is much more stable than the H^+ obtained from the cation dissociation. Therefore, region III extends to larger distances in $(F\cdots H)^+$ than in (F···H) and $(F\cdots H)^-$, as the covalent bond is preferred to the unfavorable closed-shell interaction in the former.

5. Energetic Properties at the Bond Critical Point

The local electron kinetic (G) and potential (V) energies at BCP follow trends similar to the parallel and perpendicular curvatures, mainly in the closed-shell region (Figure 6), as observed in our other preceding works. While the local potential energy presents only small differences in the intermediate region for the three systems, the local kinetic energy shows a broad peak situated at 1.35 Å for $(F\cdots H)^-$, which represents the border between regions II and III for this system. This feature, not observed in the other two cases, produces important differences between G^- and G^0, which rise up to 520 kJ/mol/Å^3 at $d =$ 1.45 Å. Out of this peak, in the shortest and largest distance ranges, both dependences are very similar.

For closed-shell interactions, the correspondence between the topological curvature λ_3 and the local kinetic energy density G has been already pointed out.[6,10] As in the case of $\lambda_3{}^-$, the G^- dependence shows that the charge depletion in the bonding region is larger for $(F\cdots H)^-$ as a consequence of the antibonding electron. Indeed, compared to G^0, the behavior of G^- indicates that the influence of the 4σ electron on BMO is significant in region II, producing an important rising of the electron kinetic energy and the concomitant charge depletion. In region III, where the molecular orbital populations are expected to remain stable, the influence of the antibonding electron is less important as the internuclear distance shortens, disappearing completely for the shortest geometries. On the other side, the G^+ magnitudes are smaller than those of G^- and G^0 for all distances. In particular, $G^+ < G^0$ points to the fact that the $(F\cdots H)^+$ system slows down the movement of electrons in BMO due to a weaker repulsion with those in the π nonbonding orbitals.

Balancing the G and V contributions, the total electron energy density at BCP ($H = G + V$) permits to identify the geometries associated with a local excess of either G or V at the interatomic surface (Figure 7). As previously reported,[10] the internuclear distance $d(H{=}0)$ is related to the starting formation of the BMO. For the three studied systems, we observe $d(H^0 = 0) < d(H^-{=}0) < d(H^+{=}0)$ (Table 1). The comparison between the (F···H) and $(F\cdots H)^+$ systems shows $H^+ < H^0$ within the full range of distances, indicating that the removal of one electron from the π nonbonding orbitals implies the concomitant gain in stabilization of the electron distribution at the interatomic surface. On the other hand, a similar comparison between (F···H) and $(F\cdots H)^-$ shows $H^0 < H^-$ for $0.92 < d < 1.85$ Å. In this case, the addition of one electron to the antibonding orbital increases H and leads to a diminution in the stabilization of the bonding charge at the interatomic surface for geometries ranging from the starting BMO^0 formation up to the equilibrium geometry $d_{eq}{}^0$.

As previously pointed out, the comparison between the H^0, H^-, and H^+ magnitudes at the equilibrium geometries ($H^0(d_{eq}{}^0) < H^-(d_{eq}{}^-) < H^+(d_{eq}{}^+)$) indicates the deepest energetic stabilization of the bonding charge at the interatomic surface for the unperturbed system, paralleling its more stable configuration. On the other side, the opposite is observed when the systems are compared at $d_{eq}{}^0$ ($H^+(d_{eq}{}^0) < H^-(d_{eq}{}^0) < H^0(d_{eq}{}^0)$), and this feature points the smallest negative magnitude of H as corresponding to the energetic characteristic of the unperturbed electron configuration at its equilibrium geometry. Both trends seem to be the energetic signature at the interatomic surface of the most stable electron configuration. In particular, the correspondence between the smallest H magnitude in region III ($H < 0$) and the most stable relaxed configuration parallels with the result observed in the theoretical analysis of the FH···FH complex,[10] where the maximum positive magnitude of H in region I ($H > 0$) was found to be associated with the equilibrium geometry of the system.

6. Conclusions

Within the framework of the MO theory, the addition of one antibonding electron to or the removal of one nonbonding electron from the neutral (F···H) system, leading to $(F\cdots H)^-$ and to $(F\cdots H)^+$, has permitted the investigation of these charge perturbations on the bond properties of the hydrogen fluoride molecule by using the topological analysis of $\rho(\mathbf{r})$. For the three systems, the dependence of the BCP topological and energetic properties on the F···H internuclear distance has been related to the corresponding behavior of the 3σ BMO distribution, which recovers BCP and results from its interaction with the average Coulomb and exchange potential generated by the charge filling the π and 4σ MOs.

This study has shown the correspondence between the calculated BCP properties and the perturbation on the bonding charge within the full range of internuclear distances. The observed behaviors suggest that important effects in the bonding region of $(F\cdots H)^-$ are both a fewer quantity and a locally more depleted electron distribution than in the case of (F···H), even if the starting BMO formation exhibits earlier in the former ($d^0(H^0=0) < d^-(H^-=0)$). On the other side, the vertical ionization of the neutral system implies the formation of the BMO at larger interaction geometries than in both (F···H) and $(F\cdots H)^-$ ($d^0(H^0=0) < d^-(H^-=0) < d^+(H^+=0)$) due to a much more unfavorable H^+ dissociation in $(F\cdots H)^+$ than that of the H-atom in (F···H) or $(F\cdots H)^-$. As a consequence, the bonding charge is locally more concentrated at the interatomic surface in $(F\cdots H)^+$ than in (F···H) ($\nabla^2\rho^+ < \nabla^2\rho^0$) for all geometries. In addition, the perturbations produce a reorganization of the electron distribution that is revealed by $\rho^0 > \rho^- > \rho^+$ within the full range of internuclear distances and by large variations in several topological and energetic properties evaluated at BCP, namely, $\nabla^2\rho$, λ_3, and G.

The E_{int} local minima calculated for (F···H), $(F\cdots H)^-$, and $(F\cdots H)^+$ indicate that the applied perturbations on the neutral system do not break the F−H bond but soften it ($E_{int}{}^0 < E_{int}{}^+ < E_{int}{}^-$). At the equilibrium geometries of these systems, the BMO formation is completed with two electrons in all cases and the comparison of their corresponding BCP properties inform about the differences between their relaxed BMO distributions at the interatomic surface. Accordingly, the specificity of the (F···H), $(F\cdots H)^-$, and $(F\cdots H)^+$ bonding properties is fundamentally characterized by the BMO polarization along the bond path direction, which leads to the particular BMO contribution at BCP. The calculation of the relative position of BCP with respect to the middle of the equilibrium geometry found for each system indicates that (i) the BMO^+ is contracted toward the F-nucleus and (ii) the BMO^- expands toward both nuclei when compared to BMO^0. In the former case, the BMO contraction corresponds to the fluorine atomic basin expansion and therefore to the BCP displacement toward the H^+-nucleus, leading to $\rho^0(d_{eq}{}^0) > \rho^+(d_{eq}{}^+)$. In the second case, the relative position of BCP from the middle of the relaxed geometry does not change from (F···H) to $(F\cdots H)^-$, indicating an approximately symmetrical BMO expansion toward both nuclei in the latter system due to its longer internuclear distance. Thus, since the BMO population is similar for both of them (i.e., two electrons), the lengthening of the $(F\cdots H)^-$ geometry leads to a diminution of the electron density along the internuclear region, and in particular at BCP ($\rho^0(d_{eq}{}^0) > \rho^-(d_{eq}{}^-)$). Hence, paralleling the quantity of bonding charge at the interatomic surface $\rho^0(d_{eq}{}^0) > \rho^-(d_{eq}{}^-) > \rho^+(d_{eq}{}^+)$, we observe the equilibrium geometries classification $d_{eq}{}^0 < d_{eq}{}^- < d_{eq}{}^+$, where both perturbed systems exhibit longer distances than the neutral one.

As a consequence of the BMO polarizations in $(F\cdots H)^+$ and in $(F\cdots H)^-$, the local concentration of the bonding charge and the total electron energy density at the interatomic surface show a dependence on the charge perturbation similar to that found for ρ ($|\nabla^2\rho^0(d_{eq}{}^0)| > |\nabla^2\rho^-(d_{eq}{}^-)| > |\nabla^2\rho^+(d_{eq}{}^+)|$, and $|H^0(d_{eq}{}^0)| > |H^-(d_{eq}{}^-)| > |H^+(d_{eq}{}^+)|$). Thus, comparing the electron density distribution of the three systems at their equilibrium geometries, the most stable configuration (i.e., that corresponding to the neutral system) is identified as that which exhibits (i) the highest quantity, (ii) the most locally concentrated, and (iii) the deepest energetically stabilized bonding charge distribution at the interatomic surface. On the other hand, if the comparison between the three systems is carried out at the equilibrium geometry of the unperturbed (F···H) system, its electron distribution shows (i) the largest quantity of bonding charge and (ii) the smallest negative magnitude of the total electron energy density H at the interatomic surface. Hence, being the signature of the most stable configuration, the characteristic magnitudes of the neutral system $\rho(d_{eq}{}^0)$, $\nabla^2\rho(d_{eq}{}^0)$, and $H(d_{eq}{}^0)$ appear as boundary conditions at the interatomic surface of its unperturbed and relaxed electron distribution.

Acknowledgment. This work has been partially supported by the Generalitat de Catalunya (Grant 2001SGR-335). E.E. thanks Prof. R. Guilard for supporting the development of a part of this work at the LIMSAG laboratory.

Supporting Information Available: Interaction energies and BCP topological and energetic properties calculated for the $(F\cdots H)^+$, (F···H), and $(F\cdots H)^-$ systems within the range of 0.8−3.0 Å of F···H distances (Table S1) and dependences of $E_{int}{}^0$, $E_{int}{}^-$, and $E_{int}{}^+$ on the d(F···H) distance (Figure S1) (6 pages). This material is available free of charge via the Internet at http://pubs.acs.org.

References and Notes

(1) An equivalent scheme has been demonstrated for nuclear matter in refs 2 and 3.

(2) Petkov, I. Zh.; Soitsov, M. V. *Oxford Studies in Nuclear Physics*; Clarendon Press: Oxford, U.K., 1991.

(3) Soubbotin, V. B.; Tselyaev, V. I.; Viñas, X. *Phys. Rev. C* **2003**, *67* (1−14), 14324.

(4) Bader, R. F. W. *Atoms in Molecules*—A Quantum Theory; Oxford University Press: Oxford, U.K., 1990.

(5) Espinosa, E.; Molins, E.; Lecomte, C. *Chem. Phys. Lett.* **1998**, *285*, 170.

(6) Espinosa, E.; Lecomte, C.; Molins, E. *Chem. Phys. Lett.* **1999**, *300*, 745.

(7) Espinosa, E.; Souhassou, M.; Lachekar, H.; Lecomte, C. *Acta Crystallogr.* **1999**, *B55*, 563.

(8) Espinosa, E.; Molins, E. *J. Chem. Phys.* **2000**, *113*, 5686.

(9) Espinosa, E.; Alkorta, I.; Rozas, I.; Elguero, J.; Molins, E. *Chem. Phys. Lett.* **2001**, *336*, 457.

(10) Espinosa, E.; Alkorta, I.; Elguero, J.; Molins, E. *J. Chem. Phys.* **2002**, *117*, 5529.

(11) NIST Standard Reference Database Number 69, March, 2003 Release. http://webbook.nist.gov/chemistry/ and therein cited references.

(12) Yencha, A. J.; Lopes, M. C. A.; King, G. C.; Hochlaf, M.; Songe, Y.; Ng, C. Y. *Faraday Discuss.* **2000**, *115*, 355.

(13) Cremer, D.; Kraka, E. *Croat. Chem. Acta* **1984**, *57*, 1259.

(14) Bader, R. F. W.; Popelier, P. L. A.; Keith, T. A. *Angew. Chem., Int. Ed. Engl.* **1994**, *33*, 620.

(15) Alkorta, I.; Elguero, J.; Espinosa, E.; Mata, I.; Molins, E. *J. Comput. Chem.* **2003**, *24*, 416.

(16) Chamorro, E.; Fuentealba, P.; Savin, A. *J. Comput. Chem.* **2003**, *24*, 496.

(17) Carroll, M. T.; Bader, R. F. W. *Mol. Phys*. **1988**, *65*, 695.
(18) Wiberg, K. B.; Rablen, P. R. *J. Comput. Chem*. **1993**, *14*, 1504.
(19) Shiga, M.; Aiga, F.; Sasagane, K. *Int. J. Quantum Chem*. **1999**, *71*, 251.
(20) Hegarty, D.; Robb, M. A. *Mol. Phys.* **1979**, *38*, 1795.
(21) Schmidt, M. W.; Baldridge, K. K.; Boatz, J. A.; Elbert, S. T.; Gordon, M. S.; Jensen, J. H.; Koseki, S.; Matsunaga, N.; Nguyen, K. A.; Su, S.; Windus, T. L.; Dupuis, M.; Montgomery J. A. *J. Comput. Chem.* **1993**, *14*, 1347.
(22) Mulliken, R. S. *Rev. Mod. Phys*. **1932**, *4*, 1.
(23) Mulliken, R. S. *Phys. Rev.* **1939**, *56*, 778.
(24) Cade, P. E.; Bader,, R. F. W.; Pelletier, J. *J. Chem. Phys*. **1971**, *54*, 3517.